ACADEMIC PRESS

Available online at www.sciencedirect.com
SCIENCE DIRECT®

Journal of Solid State Chemistry 172 (2003) 370–380

JOURNAL OF SOLID STATE CHEMISTRY

http://elsevier.com/locate/jssc

Systems *Ln*–Fe–O (*Ln* = Eu, Gd): thermodynamic properties of ternary oxides using solid-state electrochemical cells

S.C. Parida,* S.K. Rakshit, S. Dash, Ziley Singh, R. Prasad, and V. Venugopal

Fuel Chemistry Division, Bhabha Atomic Research Centre, Trombay, Mumbai 400 085, India

Received 16 July 2002; received in revised form 11 November 2002; accepted 19 November 2002

Abstract

The standard molar Gibbs energies of formation of $LnFeO_3$(s) and $Ln_3Fe_5O_{12}$(s) where *Ln* = Eu and Gd have been determined using solid-state electrochemical technique employing different solid electrolytes. The reversible e.m.f.s of the following solid-state electrochemical cells have been measured in the temperature range from 1050 to 1255 K.

Cell (I): (−)Pt / {$LnFeO_3$(s) + Ln_2O_3(s) + Fe(s)} // YDT/CSZ // {Fe(s) + $Fe_{0.95}O$(s)} / Pt(+);

Cell (II): (−)Pt/{Fe(s) + $Fe_{0.95}O$(s)}//CSZ//{$LnFeO_3$(s) + $Ln_3Fe_5O_{12}$(s) + Fe_3O_4(s)}/Pt(+);

Cell (III): (−)Pt/{$LnFeO_3$(s) + $Ln_3Fe_5O_{12}$(s) + Fe_3O_4(s)}//YSZ//{Ni(s) + NiO(s)}/Pt(+);

and

Cell(IV):(−)Pt/{Fe(s) + $Fe_{0.95}O$(s)}//YDT/CSZ//{$LnFeO_3$(s) + $Ln_3Fe_5O_{12}$(s) + Fe_3O_4(s)}/Pt(+).

The oxygen chemical potentials corresponding to the three-phase equilibria involving the ternary oxides have been computed from the e.m.f. data. The standard Gibbs energies of formation of solid $EuFeO_3$, $Eu_3Fe_5O_{12}$, $GdFeO_3$ and $Gd_3Fe_5O_{12}$ calculated by the least-squares regression analysis of the data obtained in the present study are given by

$\Delta_f G^\circ_m(EuFeO_3, s)$ /kJ mol^{-1} ($\pm$ 3.2) = −1265.5 + 0.2687(T/K) (1050 ⩽ T/K ⩽ 1570),

$\Delta_f G^\circ_m(Eu_3Fe_5O_{12}, s)$/kJ mol^{-1} ($\pm$ 3.5) = −4626.2 + 1.0474(T/K) (1050 ⩽ T/K ⩽ 1255),

$\Delta_f G^\circ_m(GdFeO_3, s)$ /kJ mol^{-1} ($\pm$ 3.2) = −1342.5 + 0.2539(T/K) (1050 ⩽ T/K ⩽ 1570),

and

$\Delta_f G^\circ_m(Gd_3Fe_5O_{12}, s)$/kJ · mol^{-1} ($\pm$ 3.5) = −4856.0 + 1.0021(T/K) (1050 ⩽ T/K ⩽ 1255).

The uncertainty estimates for $\Delta_f G^\circ_m$ include the standard deviation in the e.m.f. and uncertainty in the data taken from the literature. Based on the thermodynamic information, oxygen potential diagrams for the systems Eu–Fe–O and Gd–Fe–O and chemical potential diagrams for the system Gd–Fe–O were computed at 1250 K.

Keywords: System Eu–Fe–O; System Gd–Fe–O; Gibbs energy of formation; Oxygen chemical potential; Chemical potential diagrams; Solid-state electrochemical technique

1. Introduction

The lanthanide orthoferrites $LnFeO_3$ and the lanthanide iron garnets $Ln_3Fe_5O_{12}$ have interesting magnetic properties [1–3]. Some of the orthoferrites and their substituted analogues have potential use as electrochemical sensors and cathode materials in solid oxide fuel cells. The rare-earth iron garnets are promising materials for use in magnetic recording devices. Therefore, the physico-chemical properties of these ternary oxides are important for their practical applications. The crystal structures and magnetic properties of these compounds have been thoroughly investigated by many researchers. However, the thermodynamic properties of these oxides have been studied to a limited extent only. Quantitative information on the thermodynamic properties of these oxides are required for better understanding of their thermophysical properties and to predict their stability in different chemical environments. As a part of systematic studies on thermodynamic properties of ternary oxides in the system *Ln*–Fe–O, where *Ln* is a rare-earth element, measurements have been made on the system *Ln*–Fe–O for *Ln* = Eu and Gd.

Katsura et al. [4] have established the phase diagram of the system Ln_2O_3–Fe_2O_3–Fe at high temperature and

*Corresponding author. Fax: 91-22-550-5151.
E-mail address: sureshp@apsara.barc.ernet.in (S.C. Parida).

0022-4596/03/$ - see front matter © 2003 Elsevier Science (USA). All rights reserved.
doi:10.1016/S0022-4596(03)00008-2

reported the existence of two ternary oxides, $LnFeO_3$(s) and $Ln_3Fe_5O_{12}$(s). It is evident from their study [4] that two types of three-phase equilibria prevails at 1273 K for the systems Ln = Eu and Gd; the perovskite-type compound $LnFeO_3$(s) is in equilibrium with Fe(s) and Ln_2O_3(s) where as the garnet-type compound $Ln_3Fe_5O_{12}$(s) coexists with $LnFeO_3$(s) and Fe_3O_4(s). Katsura et al. [5] have calculated the Gibbs energies of formation of $LnFeO_3$(s) from the measured equilibrium oxygen partial pressure over the co-existing phases $LnFeO_3(s) + Ln_2O_3(s) + Fe(s)$ in the temperature range from 1473 to 1548 K using gas equilibrium technique. Katsura et al. [4] have used the same technique to measure the Gibbs energies of formation of $Ln_3Fe_5O_{12}$(s) in the temperature range from 1273 to 1473 K. In the present study, the standard molar Gibbs energies of formation of $LnFeO_3$(s) and $Ln_3Fe_5O_{12}$(s) have been calculated from the e.m.f. data obtained using solid-state galvanic cells employing different types of oxide solid electrolytes. Other thermodynamic quantities are also evaluated from the experimental data.

2. Experimental

Stoichiometric proportion of Ln_2O_3(s) (LEICO Industries Inc., 0.9985 mass fraction) and $Fe(NO_3)_3 \cdot 9H_2O$(s) (Qualigens Fine Chemicals, 0.99 mass fraction) were dissolved in dilute HNO_3. Excess amount of citric acid (E. Merck, India, 0.995 mass fraction) was added to the solution to assist in complete dissolution. The solution was heated on a hot plate around 375 K to remove water and oxides of nitrogen. A gel was formed which was heated at 450 K to dryness. The residue was ground in an agate mortar and heated at 1275 K in dry air for 48 h. The products were exclusively identified as $LnFeO_3$(s) and $Ln_3Fe_5O_{12}$(s) by X-ray diffraction (XRD) analysis using a DIANO X-ray diffractometer with Cu$K\alpha$ radiation using graphite monochromator. The particle size of $LnFeO_3$(s) and $Ln_3Fe_5O_{12}$(s) were estimated to be in the range of 2–4 μm from X-ray line broadening.

Phase mixtures $\{LnFeO_3(s) + Ln_2O_3(s) + Fe(s)\}$, $\{Ln_3Fe_5O_{12}(s) + LnFeO_3(s) + Fe_3O_4(s)\}$, $\{Fe(s) + Fe_{0.95}O(s)\}$ and $\{Ni(s) + NiO(s)\}$ in the molar ratios of (2:1:2), (3:9:2), (1:1) and (1:1) respectively, were made using a steel die at a pressure of 100 MPa for the e.m.f. measurements. The pellets were sintered in purified argon gas atmosphere ($p(O_2) \cong 10^{-18}$ bar) at 1000 K for 72 h. The argon gas was purified by passing it through towers containing the reduced form of BASF catalyst, molecular sieves, magnesium perchlorate, and hot uranium metal at 550 K. The oxygen partial pressure in the purified argon gas was calculated from the measured e.m.f. of the cell: (−) Pt/{Ar(g), $p(O_2) = x$ bar)}//CSZ//O_2(g), 1.01325 bar/Pt (+). The calculated value of x is ($p(O_2) \cong 10^{-18}$ bar) at 1000 K. The sintered pellets were reexamined by XRD method and the phase compositions were found unchanged after sintering.

2.1. Solid-state electrochemical technique

The experimental details and the cell assembly used for e.m.f. measurements have been reported earlier [6]. A double compartment cell assembly was used. The inner compartment was separated from the outer compartment by the use of electrolyte tubes. The electrolyte tube separated the gas phase over the two electrodes so that transport of oxygen from the higher oxygen potential electrode to the lower oxygen potential electrode via the gas phase is prevented. The yttria-stabilized zirconia (YSZ) electrolyte with 6 mol% Y_2O_3 was supplied by Karatec Advanced Materials SA, Spain where as the calcia-stabilized zirconia (CSZ) electrolyte tube with 15 mol% CaO was supplied by Nikatto Corporation, Japan. The dimensions of both the YSZ and CSZ electrolyte tubes were; 13 mm o.d., 9 mm i.d., and 380 mm long with a flat closed end. It has been reported by Pratt [7] that the range of permissible oxygen partial pressures for purely ionic conduction for CSZ electrolyte is about 10^{-25} bar at 1000 K and 10^{-18} bar at 1273 K. YSZ electrolyte has similar range of oxygen partial pressure and temperature for purely ionic conduction. However, for a typical 7.5 mol% YDT (yttria-doped thoria) electrolyte, measurements may normally be made down to oxygen partial pressure of 10^{-37} bar at 1000 K and 10^{-30} bar at 1273 K [7]. An alternative procedure for extending the measurement range for low oxygen partial pressure has been discussed by Shores and Rapp [8]. According to their experiment [8], a bielectrolyte cell involving the solid electrolyte combination YDT/CSZ can extend the electrolytic conduction domain over that of the single CSZ electrolyte. It has been estimated in the present study that the oxygen partial pressure prevailing over the three-phase mixture $LnFeO_3(s) + Ln_2O_3(s) + Fe(s)$ is about 10^{-23} bar at 1000 K where as that for the three-phase mixture $Ln_3Fe_5O_{12}(s) + LnFeO_3(s) + Fe_3O_4(s)$ is about 10^{-20} bar at 1000 K. It is evident from the present estimation that the oxygen partial pressure over the phase mixture $LnFeO_3(s) + Ln_2O_3(s) + Fe(s)$ is near the boundary of the purely ionic conduction domain for CSZ or YSZ electrolyte. It is unwise to use either CSZ or YSZ electrolyte for the measurement of oxygen chemical potential over this phase mixture. Hence, in the present study a bi-electrolyte cell assembly involving the electrolyte combination YDT/CSZ has been used for measurements over the three-phase mixture $LnFeO_3(s) + Ln_2O_3(s) + Fe(s)$. The bi-electrolyte cell was arranged in such a way that the YDT electrolyte (in the form of a disc, Supplied by Bhabha Atomic Research Centre, India) was adjacent to the electrode having low oxygen chemical potential. This ensured that

the transport number of oxygen ion was close to unity for the solid electrolyte combination [8]. However, the estimated oxygen partial pressures over the three-phase mixture $Ln_3Fe_5O_{12}(s) + LnFeO_3(s) + Fe_3O_4(s)$ are within the electrolytic conduction domain of CSZ or YSZ electrolytes and hence the measurements can be safely done using these electrolytes. Though a bielectrolyte cell is not going to give any added advantage in this case, it has been used in the present case to confirm the validity of its use. An inert environment was maintained over the solid electrodes throughout the experiment by streams of purified argon gas. The argon gas was purified by passing it through towers containing the reduced form of BASF catalyst, molecular sieves, magnesium perchlorate and hot uranium metal at 550 K. The cell temperature (± 1 K) was measured by a calibrated chromel/alumel thermocouple (ITS-90), and the cell e.m.f. (± 0.02 mV) by a Keithley 614 electrometer (impedance $> 10^{14}\,\Omega$). The reversible e.m.f.s of the following solid-state galvanic cells were measured as a function of temperature.

Cell (I): $(-)Pt/\{LnFeO_3(s) + Ln_2O_3(s) + Fe(s)\}//YDT/CSZ//\{Fe(s) + Fe_{0.95}O(s)\}/Pt(+)$,

Cell (II): $(-)Pt/\{Fe(s) + Fe_{0.95}O(s)\}//CSZ//\{Ln_3Fe_5O_{12}(s) + LnFeO_3(s) + Fe_3O_4(s)\}/Pt(+)$,

Cell (III): $(-)Pt/\{Ln_3Fe_5O_{12}(s) + LnFeO_3(s) + Fe_3O_4(s)\}//YSZ//\{Ni(s) + NiO(s)\}/Pt(+)$,

Cell (IV): $(-)Pt/\{Fe(s) + Fe_{0.95}O(s)\}//YDT/CSZ//\{Ln_3Fe_5O_{12}(s) + LnFeO_3(s) + Fe_3O_4(s)\}/Pt(+)$.

E.m.f. measurements were carried out in the temperature range 1050–1255 K. The reversibility of the solid-state electrochemical cells was checked by microcoulometric titration in both directions. A small quantity of current is passed ($\sim 100\,\mu A$ for ~ 10 min) through the cell in either direction. After the removal of applied voltage, the cell e.m.f. returned to its original value. The e.m.f. of cells were also found to be independent of flow rate of the inert gas passing over the electrodes in the range from 2 to 6 ml min^{-1}. The X-ray diffraction patterns of the pellets before and after experiments were found unchanged.

3. Results and discussion

3.1. Solid-state electrochemical measurements

The e.m.f. of the solid oxide galvanic cell is related to the partial pressure of oxygen at the two electrodes by the relation

$$E = (RT/nF)\int_{p''(O_2)}^{p'(O_2)} t(O^{2-})\mathrm{d}\ln p(O_2), \quad (1)$$

where E is the measured e.m.f. of the cell in volts, R ($=8.3144\,J\,K^{-1}\,mol^{-1}$) is the universal gas constant, n ($=4$) is the number of electrons participating in the electrode reaction, $F(=96486.4\,C\,mol^{-1})$ is the Faraday constant, T is the absolute temperature, $t(O^{2-})$ is the effective transference number of O^{2-} ion for the solid electrolyte combination, and $p'(O_2)$ and $p''(O_2)$ are the equilibrium oxygen partial pressures at the positive and negative electrodes, respectively. The transport number of oxygen ion in the solid electrolytes used in the present study is nearly unity ($t(O^{2-}) > 0.99$) at the oxygen pressures and temperatures covered. Hence, the e.m.f. of the cell is directly proportional to the logarithm of the ratio of partial pressures of oxygen at the electrodes

$$E = (RT/4F)\ln\{p'(O_2)/p''(O_2)\}. \quad (2)$$

Thus,

$$4FE = RT\ln p'(O_2) - RT\ln p''(O_2), \quad (3)$$

where, $RT\ln p'(O_2)$ is the oxygen potential over the cathode and $RT\ln p''(O_2)$ is the oxygen chemical potential corresponding to the anode.

3.2. System Eu–Fe–O

3.2.1. Oxygen chemical potential over the three-phase electrode $\{EuFeO_3(s)+Eu_2O_3(s)+Fe(s)\}$

The reversible e.m.f. of cell (I) for $Ln = Eu$ are listed in Table 1. Variation of the e.m.f. as a function of temperature for cell (I) is shown in Fig. 1. The e.m.f. data were least-squares fitted to give the relations

$$\mathrm{Cell(I)}: E/V(\pm 0.0004) = 0.1642 - 8.197\times 10^{-5}(T/K). \quad (4)$$

The oxygen chemical potential corresponding to three-phase mixtures $\{EuFeO_3(s) + Eu_2O_3(s) + Fe(s)\}$ have been calculated using Eq. (3), the values of $\Delta\mu(O_2)$ for the phase mixture $\{Fe(s) + Fe_{0.95}O(s)\}$ from Sundman [9] and the values of e.m.f. obtained in the present study. For the equilibrium reaction

$$2/3Eu_2O_3(s) + 4/3Fe(s) + O_2(g) = 4/3EuFeO_3(s) \quad (5)$$

the results obtained can be represented by the following equation:

$$\Delta\mu(O_2)/kJ\,mol^{-1}(\pm 0.5) = -591.1 + 0.1611(T/K) \quad (1052 \le T/K \le 1253). \quad (6)$$

Katsura et al. [5] have measured the equilibrium oxygen chemical potential for reaction [5] in the temperature range from 1473 to 1570 K using the gas equilibration technique involving CO_2–H_2 gas mixtures. The values of $\Delta\mu(O_2)$ obtained in the present study are compared with those obtained by Katsura et al. [5] in Fig. 2. It is apparent that the results obtained in this study when extrapolated to higher temperatures are in fair agreement with those reported by Katsura et al. [5]. It has been decided therefore to calculate the values of $\Delta\mu(O_2)$ in the whole temperature range from 1050 to

Table 1
The reversible e.m.f. of cells (I)–(IV) for $Ln = Eu$

Cell (I)		Cell (II)		Cell (III)		Cell (IV)	
T/K	E/V	T/K	E/V	T/K	E/V	T/K	E/V
1052	0.0772	1050	0.0629	1053	0.2024	1052	0.0610
1077	0.0761	1062	0.0672	1068	0.1992	1064	0.0660
1098	0.0745	1080	0.0735	1081	0.1975	1081	0.0733
1107	0.0736	1100	0.0792	1103	0.192	1101	0.0799
1115	0.0733	1118	0.0847	1123	0.1863	1122	0.0864
1120	0.0725	1122	0.0854	1128	0.1862	1140	0.0920
1142	0.0698	1141	0.0914	1155	0.1794	1161	0.0986
1152	0.0695	1160	0.0975	1180	0.1752	1178	0.1037
1163	0.0692	1186	0.1059	1205	0.1701	1198	0.1102
1174	0.0678	1209	0.1151	1229	0.1650	1215	0.1157
1202	0.0656	1236	0.1231	1241	0.1619	1234	0.1216
1212	0.0652	1253	0.1281	1252	0.1596	1248	0.1255
1226	0.0634						
1253	0.0613						

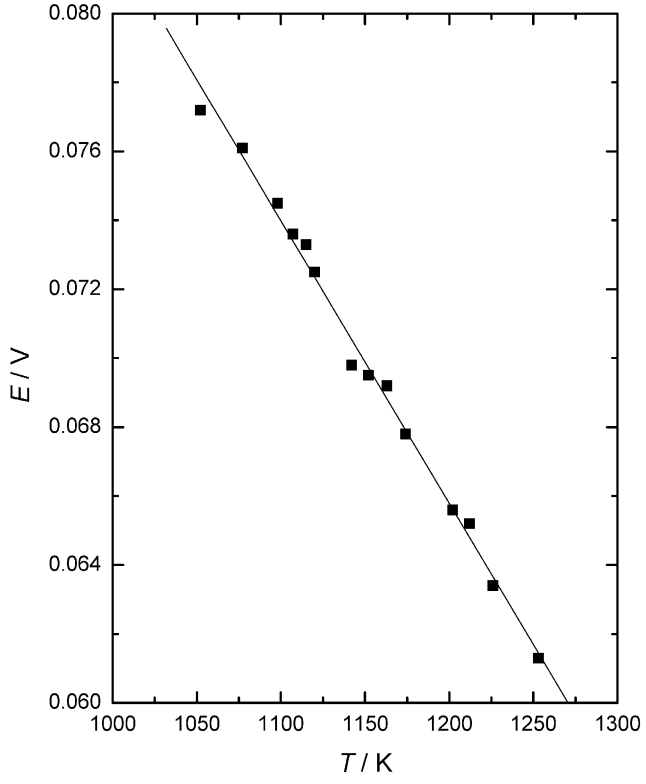

Fig. 1. Variation of e.m.f. as a function of temperature for cell (I). (−) Pt/{$EuFeO_3$(s) + Eu_2O_3(s) + Fe(s)}//YDT/CSZ//{Fe(s) + $Fe_{0.95}O$(s)}/Pt(+).

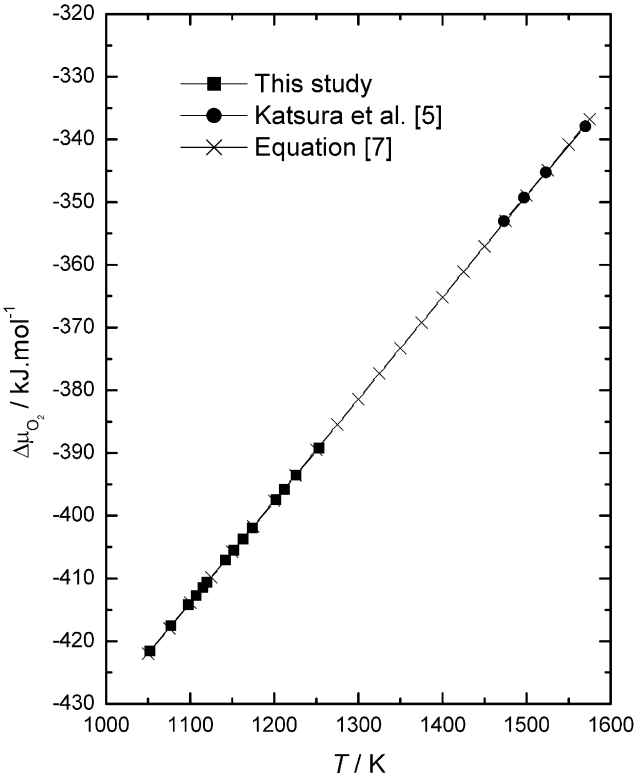

Fig. 2. Comparison of values of $\Delta\mu(O_2)$ for the reaction, 2/3 Eu_2O_3(s) + 4/3 Fe(s) + O_2(g) = 4/3 $EuFeO_3$(s).

1570 K by least-squares regression analysis of both sets of data. The values calculated thus are given by

$$\Delta\mu(O_2)/\text{kJmol}^{-1}(\pm 1.2) = -592.4 + 0.1623(T/\text{K}) \quad (1050 \le T/\text{K} \le 1570). \tag{7}$$

The values of $\Delta_f G^\circ_m(EuFeO_3,s)$ have been obtained using Eq. (7) and $\Delta_f G^\circ_m(Eu_2O_3,s)$ from Barin [10]. The standard molar Gibbs energy of formation of $EuFeO_3$(s) from elements is given by

$$\Delta_f G^\circ_m(EuFeO_3, s)/\text{kJ mol}^{-1}(\pm 1.8) = -1265.5 + 0.2687(T/\text{K}). \tag{8}$$

The temperature independent and temperature dependent terms in Eq. (8) correspond to $\Delta_f H^\circ_m(T_{av})$ and $\Delta_f S^\circ_m(T_{av})$, respectively, with $T_{av}/K = 1310$. The standard Gibbs energy of formation of $EuFeO_3$(s) from

its component oxides $Eu_2O_3(s)$ and $Fe_2O_3(s)$ in the temperature range 1050–1570 K have been obtained by combining Eq. (8) with data for $Fe_2O_3(s)$ taken from Ref. [9]. According to the reaction

$$1/2Eu_2O_3(s) + 1/2Fe_2O_3(s) = EuFeO_3(s) \quad (9)$$

the standard Gibbs energy of formation of $EuFeO_3(s)$ from its component oxides are given by

$$\Delta_{ox}G^{\circ}{}_m/\mathrm{kJmol}^{-1}(\pm 2.4) = -41.9 - 0.0007(T/\mathrm{K}). \quad (10)$$

3.2.2. *Oxygen chemical potential over the three-phase electrode* $\{Eu_3Fe_5O_{12}(s)+EuFeO_3(s)+Fe_3O_4(s)\}$

The reversible e.m.f. of cells (II), (III) and (IV) for $Ln = Eu$ are listed in Table 1 and variation of the e.m.f. as a function of temperature are shown in Fig. 3. The e.m.f. data were least-squares fitted to give the relations

$$\mathrm{Cell(II)} : E/\mathrm{V}(\pm 0.0007) = -0.2739 + 3.209 \times 10^{-4}(\mathrm{T/K}), \quad (11)$$

$$\mathrm{Cell(III)} : E/\mathrm{V}(\pm 0.0006) = 0.4293 - 2.154 \times 10^{-4}(T/\mathrm{K}), \quad (12)$$

$$\mathrm{Cell(IV)} : E/\mathrm{V}(\pm 0.0009) = -0.2778 + 3.238 \times 10^{-4}(T/\mathrm{K}). \quad (13)$$

The oxygen chemical potential corresponding to three-phase mixture $\{Eu_3Fe_5O_{12}(s) + EuFeO_3(s) + Fe_3O_4(s)\}$ in the system Eu–Fe–O have been calculated using the values of $\Delta\mu(O_2)$ for the phase mixture $\{Fe(s) + Fe_{0.95}O(s)\}$ and $\{Ni(s) + NiO(s)\}$ from Refs. [9, 10], respectively and the values of e.m.f. obtained in the present study. For the equilibrium reaction

$$18\ EuFeO_3(s) + 4Fe_3O_4(s) + O_2(g) = 6Eu_3Fe_5O_{12}(s) \quad (14)$$

the results obtained are shown in Fig. 4. It is evident from Fig. 4 that the values of $\Delta\mu(O_2)$ for the equilibrium reaction (14) obtained from the e.m.f. measurements of cell (II), (III) and (IV) are in good agreement within $\pm 1\ \mathrm{kJmol}^{-1}$ in the temperature range from 1050 to 1255 K and hence it has been decided to calculate the values of $\Delta\mu(O_2)$ in this temperature range by least-squares regression analysis of all the three sets of data. The calculated values are given by

$$\Delta\mu(\mathrm{O2})/\mathrm{kJ\,mol}^{-1}(\pm 0.5) = -632.3 + 0.2522(T/\mathrm{K}) \quad (1050 \le T/\mathrm{K} \le 1255). \quad (15)$$

Katsura et al. [4] have measured the equilibrium oxygen chemical potential for reaction (14) at 1273, 1373, and 1473 K using the gas equilibration technique involving CO_2–H_2 gas mixtures. The values of $\Delta\mu(O_2)$

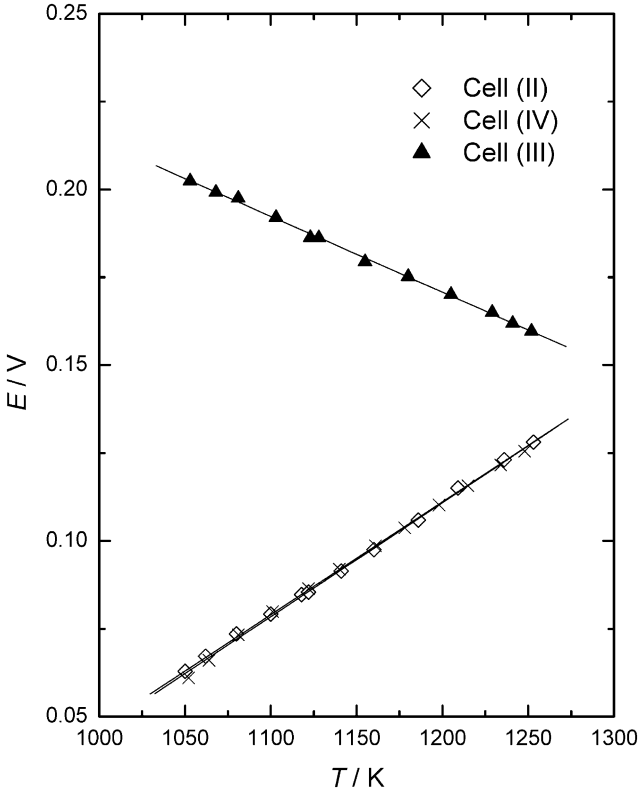

Fig. 3. Variation of e.m.f. as a function of temperature for cells (II), (III) and (IV), where $Ln = Eu$.

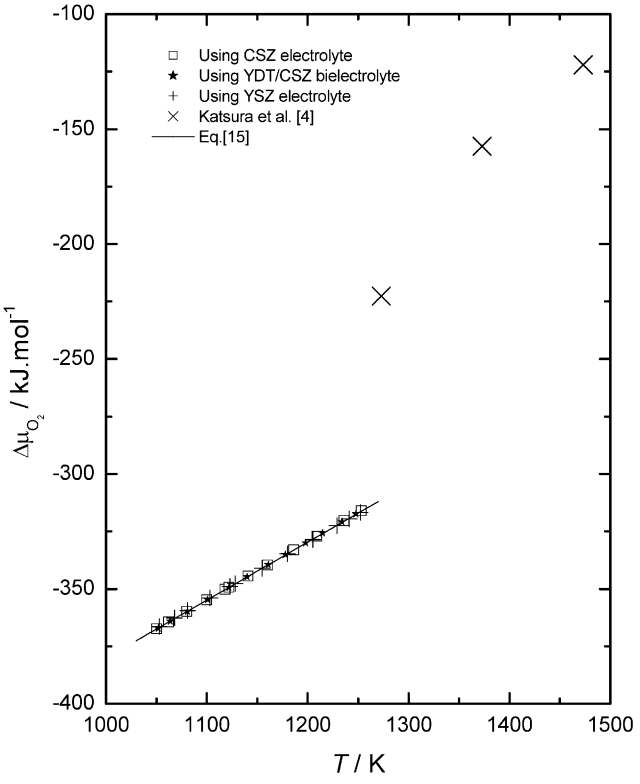

Fig. 4. Comparison of values of $\Delta\mu(O_2)$ for the reaction, 18 $EuFeO_3(s) + 4\ Fe_3O_4(s) + O_2(g) = 6\ Eu_3Fe_5O_{12}(s)$.

obtained in the present study are compared with those obtained by Katsura et al. [4] in Fig. 4. It is apparent that the results obtained in this study when extrapolated to higher temperatures are significantly lower than the values reported by Katsura et al. [4]. The slope of the oxygen chemical potential deduced from the values of Katsura et al. [4] gives an unacceptably low value ($-503\,JK^{-1}mol^{-1}$) for the partial molar entropy of oxygen in equilibrium with the three condensed phases. It is decided therefore to select the results obtained in the present study alone to calculate other thermodynamic functions.

The values of $\Delta_f G^\circ_m(Eu_3Fe_5O_{12}, s)$ have been obtained using Eq. (15), $\Delta_f G^\circ_m(EuFeO_3, s)$ from Eq. (18) and $\Delta_f G^\circ_m(Fe_3O_4, s)$ from Ref. [9]. The standard molar Gibbs energy of formation of $Eu_3Fe_5O_{12}$(s) from elements is given by

$$\Delta_{ox} G^\circ_m(Eu_3Fe_5O_{12}, s)/kJ\,mol^{-1}(\pm 2.0) = -4626.2 + 1.0474(T/K). \quad (16)$$

Standard molar enthalpy $\Delta_f H^\circ_m(T_{av.})$ and entropy of formation $\Delta_f S^\circ_m(T_{av})$ at an average temperature (T_{av}) can be obtained from the temperature independent and temperature dependent terms in Eq. (16). The standard Gibbs energy of formation of $Eu_3Fe_5O_{12}$(s) from its component oxides Eu_2O_3(s) and Fe_2O_3(s) in the temperature range 1050–1255 K have been obtained by combining Eq. (15) with data for Fe_2O_3(s) and Fe_3O_4(s) from Ref. [9]. According to the reaction

$$3/2Eu_2O_3(s) + 5/2Fe_2O_3(s) = Eu_3Fe_5O_{12}(s) \quad (17)$$

the standard Gibbs energy of formation of $Eu_3Fe_5O_{12}$(s) from its component oxides are given by

$$\Delta_{ox} G^\circ_m/kJ\,mol^{-1}(\pm 3.5) = -150.7 - 0.006(T/K). \quad (18)$$

3.3. System Gd–Fe–O

3.3.1. Oxygen chemical potential over the three-phase electrode {$GdFeO_3(s)+Gd_2O_3(s)+Fe(s)$}

The reversible e.m.f. of cell (I) for $Ln = Gd$ are listed in Table 2. Variation of the e.m.f. as a function of temperature for cell (I) is shown in Fig. 5. The e.m.f. data were least-squares fitted to give the relations

$$Cell(I): E/V(\pm 0.0002) = 0.1290 - 5.848 \times 10^{-5}(T/K). \quad (19)$$

The oxygen chemical potential corresponding to three-phase mixtures {$GdFeO_3$(s) + Gd_2O_3(s) + Fe(s)} have been calculated using the values of $\Delta\mu(O_2)$ for the phase mixture {Fe(s) + $Fe_{0.95}O$(s)} from Ref. [9] and the values of e.m.f. obtained in the present study and using Eq. (3). For the equilibrium reaction

$$2/3Gd_2O_3(s) + 4/3Fe(s) + O_2(g) = 4/3GdFeO_3(s) \quad (20)$$

the results obtained can be represented by the following equations:

$$\Delta\mu(O_2)/kJ\,mol^{-1}(\pm 0.5) = -577.5 + 0.1520(T/K) \quad (1052 \le T/K \le 1253). \quad (21)$$

The values of $\Delta\mu(O_2)$ obtained in the present study are compared with those obtained by Katsura et al. [5] in Fig. 6. The results obtained in this study when extrapolated to higher temperatures are in fair agreement

Table 2
The reversible e.m.f. of cells (I)–(IV) for $Ln = Gd$

Cell (I)		Cell (II)		Cell (III)		Cell (IV)	
T/K	E/V	T/K	E/V	T/K	E/V	T/K	E/V
1052	0.0675	1050	0.0636	1052	0.2015	1050	0.0656
1069	0.0665	1069	0.0705	1066	0.1968	1065	0.0691
1084	0.0657	1097	0.0780	1090	0.1926	1083	0.0745
1098	0.0647	1118	0.0839	1101	0.1906	1098	0.0791
1116	0.0637	1137	0.0900	1123	0.1859	1110	0.0828
1132	0.0629	1140	0.0922	1143	0.1825	1120	0.0858
1149	0.0616	1147	0.0932	1152	0.1812	1134	0.0903
1169	0.0606	1152	0.0955	1160	0.1786	1138	0.0916
1177	0.0601	1155	0.0966	1172	0.1764	1141	0.0920
1182	0.0600	1175	0.1026	1181	0.1746	1162	0.0984
1192	0.0595	1178	0.1040	1191	0.1727	1181	0.1044
1203	0.0589	1180	0.1045	1200	0.1707	1201	0.1106
1210	0.0584	1185	0.1057	1209	0.1687	1221	0.1166
1215	0.0580	1195	0.1089	1219	0.1668	1238	0.1241
1220	0.0577	1205	0.1117	1240	0.1630	1252	0.1251
1225	0.0573	1214	0.1147				
1235	0.0565	1234	0.1211				
1253	0.0557	1250	0.1259				

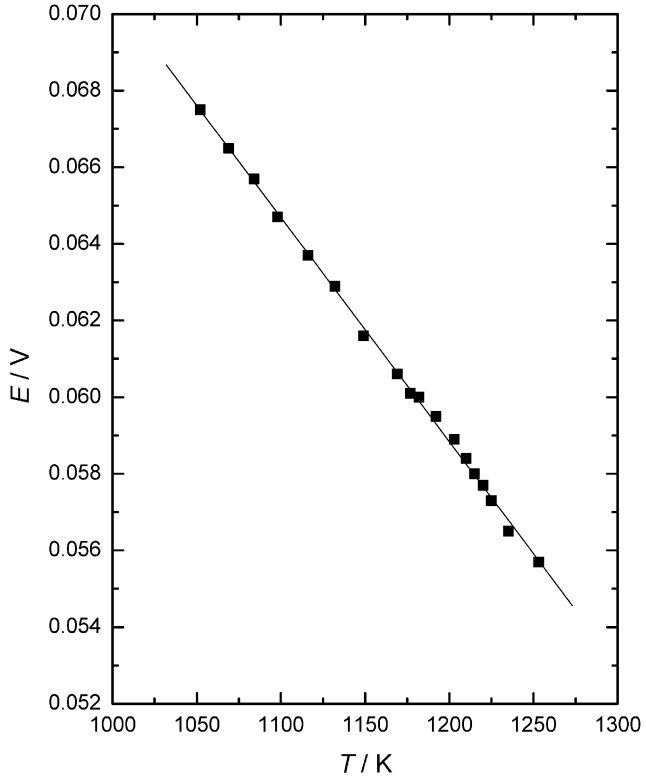

Fig. 5. Variation of e.m.f. as a function of temperature for cell (I): (−) Pt/{$GdFeO_3$(s) + Gd_2O_3(s) + Fe(s)}//YDT/CSZ//{Fe(s) + $Fe_{0.95}O$(s)}/Pt(+).

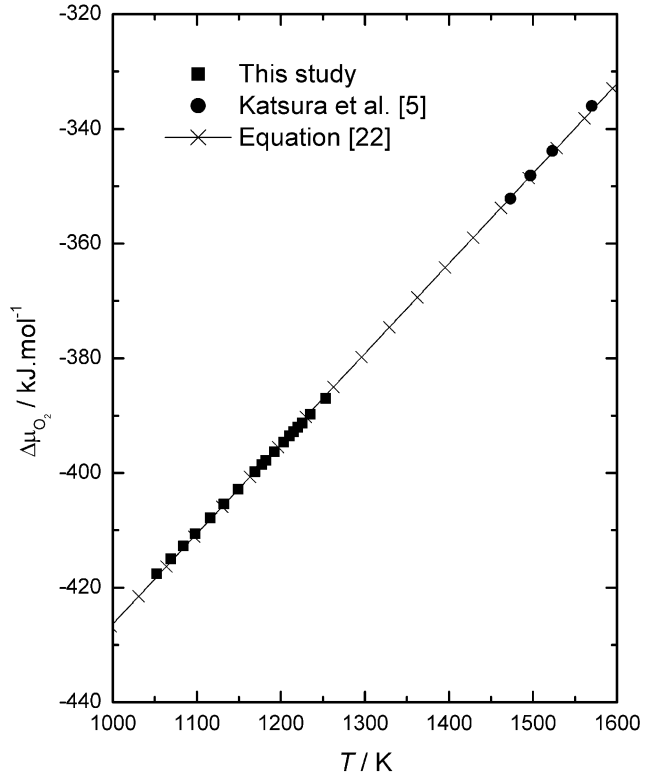

Fig. 6. Comparison of values of $\Delta\mu(O_2)$ for the reaction, $\frac{2}{3}Gd_2O_3(s) + \frac{4}{3}Fe(s) + O_2(g) = \frac{4}{3}GdFeO_3(s)$.

with those reported by Katsura et al. [5]. Hence, the values of $\Delta\mu(O_2)$ in the whole temperature range from 1050 to 1570 K have been calculated by least-squares regression analysis of both sets of data. The values calculated thus are given by

$$\Delta\mu(O_2)/\text{kJ mol}^{-1}(\pm 1.4) = -583.4 + 0.1571(T/\text{K}) \quad (1050 \le T/\text{K} \le 1570). \tag{22}$$

The values of $\Delta_f G^\circ_m(GdFeO_3,s)$ have been obtained using Eq. (22) and $\Delta_f G^\circ_m(Gd_2O_3,s)$ from Ref. [10]. The standard molar Gibbs energy of formation of $GdFeO_3$(s) from elements is given by

$$\Delta_f G^\circ_m(GdFeO_3, s)/\text{kJ mol}^{-1}(\pm 1.6) = -1342.5 + 0.2539(T/\text{K}). \tag{23}$$

The temperature independent and temperature dependent terms in Eq. (23) correspond to $\Delta_f H^\circ_m(T_{av})$ and $\Delta_f S^\circ_m(T_{av})$, respectively, with $T_{av}/\text{K} = 1310$. The standard Gibbs energy of formation of $GdFeO_3$(s) from its component oxides Gd_2O_3(s) and Fe_2O_3(s) in the temperature range 1050–1570 K have been obtained by combining Eq. (22) with data for Fe_2O_3(s) taken from Ref. [10]. According to the reaction

$$1/2Gd_2O_3(s) + 1/2Fe_2O_3(s) = GdFeO_3(s) \tag{24}$$

the standard Gibbs energy of formation of $GdFeO_3$(s) from its component oxides are given by

$$\Delta_{ox} G^\circ_m/\text{kJ mol}^{-1}(\pm 2.0) = -35.2 - 0.0046(T/\text{K}). \tag{25}$$

3.3.2. *Oxygen chemical potential over the three-phase electrode {$Gd_3Fe_5O_{12}$(s)+$GdFeO_3$(s)+Fe_3O_4(s)}*

The reversible e.m.f. of cells (II)–(IV) for Ln = Gd are listed in Table 2 and variation of the e.m.f. as a function of temperature are shown in Fig. 7. The e.m.f. data were least-square fitted to give the relations

$$\text{Cell(II)}: E/\text{V}(\pm 0.0005) = -0.2635 + 3.116 \times 10^{-4}(T/\text{K}), \tag{26}$$

$$\text{Cell(III)}: E/\text{V}(\pm 0.0005) = 0.4118 - 2.009 \times 10^{-4}(T/\text{K}), \tag{27}$$

$$\text{Cell(IV)}: E/\text{V}(\pm 0.0007) = -0.2554 + 3.048 \times 10^{-4}(T/\text{K}). \tag{28}$$

The oxygen chemical potential corresponding to three-phase mixture {$Gd_3Fe_5O_{12}$(s) + $GdFeO_3$(s) + Fe_3O_4(s)} in the system Gd–Fe–O have been calculated using the values of $\Delta\mu(O_2)$ for the phase mixture {Fe(s) + $Fe_{0.95}O$(s)} and {Ni(s) + NiO(s)} from Ref. [9,10], respectively, and the values of e.m.f. obtained in the present study. For the equilibrium reaction

$$18GdFeO_3(s) + 4Fe_3O_4(s) + O_2(g) = 6Gd_3Fe_5O_{12}(s) \tag{29}$$

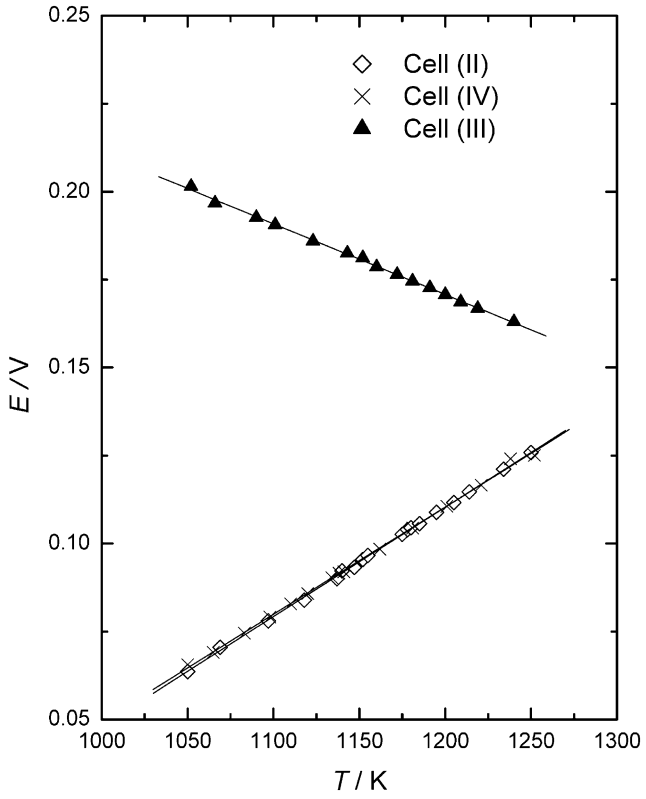

Fig. 7. Variation of e.m.f. as a function of temperature for cells (II), (III) and (IV), where Ln = Gd.

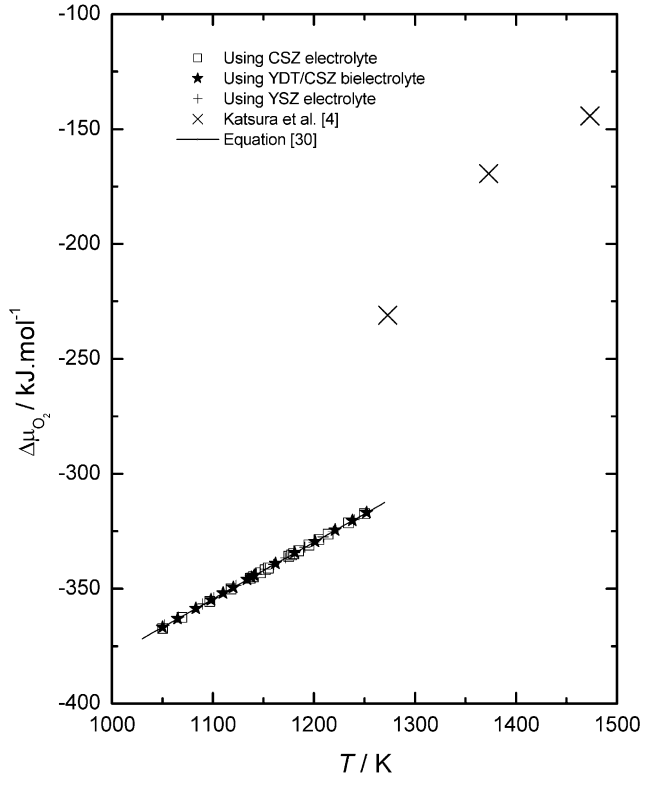

Fig. 8. Comparison of values of $\Delta\mu(O_2)$ for the reaction, $18GdFeO_3(s) + 4Fe_3O_4(s) + O_2(g) = 6Gd_3Fe_5O_{12}(s)$.

the results obtained are shown in Fig. 8. The values of $\Delta\mu(O_2)$ for the equilibrium reaction (29) obtained from the e.m.f. measurements of cell (II), (III) and (IV) are in good agreement within $\pm 1\,kJ\,mol^{-1}$ in the temperature range from 1050 to 1255 K. The values of $\Delta\mu(O_2)$ obtained by a least-squares regression analysis of all the three data sets can be given by

$$\Delta\mu(O_2)/kJ\,mol^{-1}(\pm 0.5) = -626.0 + 0.2468(T/K) \quad (1050 \le T/K \le 1255). \tag{30}$$

The values of $\Delta\mu(O_2)$ obtained in the present study are compared with those obtained by Katsura et al. [4] in Fig. 8. It is evident from Fig. 8 that the results obtained in this study when extrapolated to higher temperatures are significantly lower than the values reported by Katsura et al. [4]. The slope of the oxygen chemical potential deduced from the values of Katsura et al. [4] is abnormally low value ($-433\,JK^{-1}\,mol^{-1}$) for the partial molar entropy of oxygen in equilibrium with the three condensed phases. Therefore, it is decided to select the results obtained in the present study alone to calculate other thermodynamic functions.

The values of $\Delta_f G^\circ_m(Gd_3Fe_5O_{12}, s)$ have been obtained using Eq. (30), $\Delta_f G^\circ_m(GdFeO_3, s)$ from Eq. (23) and $\Delta_f G^\circ_m(Fe_3O_4, s)$ from Ref. [9]. The standard molar Gibbs energy of formation of $Gd_3Fe_5O_{12}(s)$ from elements is given by

$$\Delta_f G^\circ_m(Gd_3Fe_5O_{12}, s)/kJ\,mol^{-1}(\pm 2.9) = -4856.0 + 1.0021(T/K). \tag{31}$$

Standard molar enthalpy $\Delta_f H^\circ_m(T_{av})$ and entropy of formation $\Delta_f S^\circ_m(T_{av})$ at an average temperature (T_{av}) can be obtained from the temperature independent and temperature dependent terms in Eq. (31). The standard Gibbs energy of formation of $Gd_3Fe_5O_{12}(s)$ from its component oxides $Gd_2O_3(s)$ and $Fe_2O_3(s)$ in the temperature range 1050–1255 K have been obtained by combining Eq. (30) with data for $Fe_2O_3(s)$ and $Fe_3O_4(s)$ from Sundman [9]. According to the reaction

$$3/2Gd_2O_3(s) + 5/2Fe_2O_3(s) = Gd_3Fe_5O_{12}(s) \tag{32}$$

the standard Gibbs energy of formation of $Gd_3Fe_5O_{12}(s)$ from its component oxides are given by

$$\Delta_{ox} G^\circ_m/kJ\,mol^{-1}(\pm 3.8) = -129.5 - 0.0182(T/K). \tag{33}$$

3.4. Isothermal oxygen potential diagram

In ternary systems containing a volatile component such as oxygen, it is useful to visualize phase relations as a function of the chemical potential or partial pressure of the volatile species. The oxygen chemical potential of the gas phase can be readily controlled by adjusting the composition of the gas. In isothermal oxygen potential diagram the phase relations are represented as a function of partial pressure of oxygen. The composition

variable is the cationic fraction, $\eta_{Ln}/(\eta_{Ln}+\eta_{Fe})$, where η_i represents moles of component 'i'. Since oxygen is not included in the composition parameter, information on oxygen nonstoichiometry cannot be displayed in this type of diagram. Nevertheless, the diagram provides useful information on the oxygen potential range for the stability of the various phases. The diagram is complementary to the conventional Gibbs triangle representation of phase relations in ternary systems, where the composition of each phase can be unambiguously displayed. All the topological rules of construction for conventional binary temperature-composition phase diagrams are applicable to the oxygen potential diagrams. The oxygen potential diagram for the systems Eu–Fe–O and Gd–Fe–O at 1250 K, computed from the results of this study and the data for the binary systems Fe–O, Eu–O, Gd–O and Fe–Gd from Ref. [9,10,11], respectively, are shown in Figs. 9 and 10, respectively. The thermodynamic data for the system Fe–Eu is not available in the literature and hence the oxygen chemical potential corresponding the equilibria between oxides and alloys/intermetallics in the system Eu–Fe–O are not shown in Fig. 9. When three condensed phases coexist with a gas phase at equilibrium in the ternary system *Ln*–Fe–O, where *Ln* = Eu and Gd, the system is univariant; at a fixed temperature, three condensed phases coexist only at a unique partial pressure of oxygen. Therefore, horizontal lines on the diagram represent three-phase equilibrium. It is evident from Figs. 9 and 10 that on reducing the oxygen partial pressure at 1250 K, $Ln_3Fe_5O_{12}$(s) dissociates first to Fe_3O_4(s) and $LnFeO_3$(s), followed by $LnFeO_3$(s) to Fe(s) and Ln_2O_3(s). Fig. 10 shows that all the alloys and intermetallic compounds in the system Gd–Fe–O are in equilibrium with Gd_2O_3(s). The oxygen chemical potential corresponding to alloy–oxide equilibria are too low for direct measurement by experimental techniques. Similar oxygen potential diagrams at other temperatures can be readily computed from the thermodynamic data if required for a specific application.

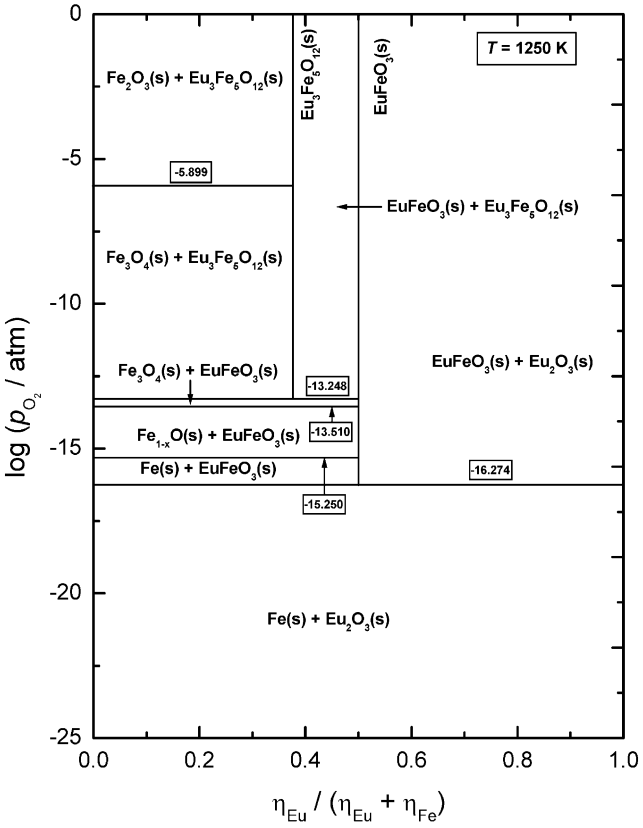

Fig. 9. Isothermal oxygen potential diagram for the system Eu–Fe–O at 1250 K. Numbers in side boxes in the figure indicate values of $\log p(O_2)$ corresponding to the lines parallel to the abscissa.

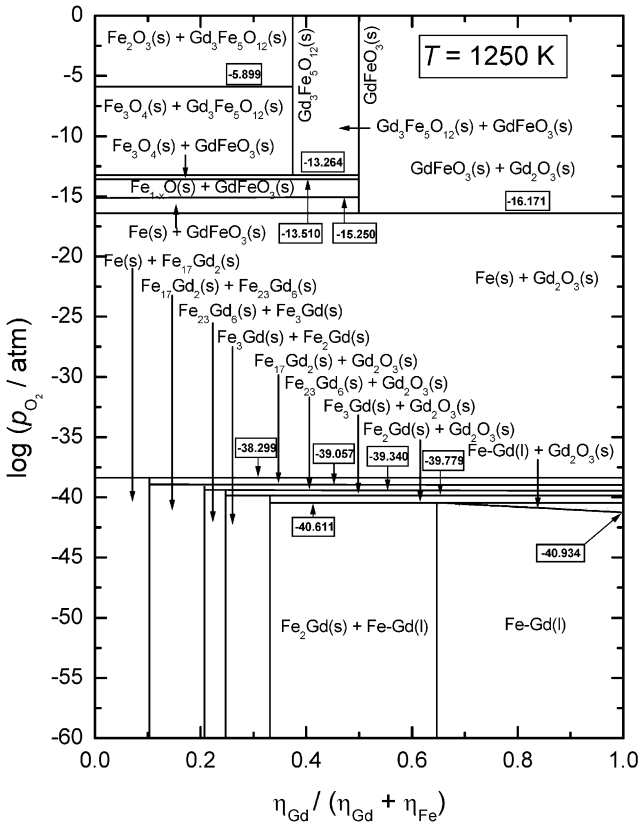

Fig. 10. Isothermal oxygen potential diagram for the system Gd–Fe–O at 1250 K. Numbers inside boxes in the figure indicate values of $\log p(O_2)$ corresponding to the lines parallel to the abscissa.

3.5. Isothermal chemical potential diagram

A major disadvantage of the oxygen potential diagram shown in Figs. 9 and 10 is that it provides no information on the chemical potentials of metallic components in different phase fields of the ternary system. This disadvantage can be overcome by choosing $\log(a_{Fe}/a_{Ln})$ and $\log p(O_2)$ as variables in a two-dimensional plot at constant temperature. The values of $\log(a_{Fe}/a_{Ln})$ can vary from plus infinity to minus infinity as pure metals or binary oxides are approached on either the *Ln*-rich side or Fe-rich side of the ternary. At actual phase boundaries

one always encounters finite values for log (a_{Fe}/a_{Ln}). In the present study, only the chemical potential diagrams for the system Gd–Fe–O have been computed using the thermodynamic data for the component binaries Fe–O, Gd–O and Fe–Gd available in the literature. The calculation method adopted here is described in detail by Yokokawa et al. [12, 13]. Each phase is represented by a polygon. The boundaries between two phases can be derived from thermodynamic data. Assume two phases $Gd_lFe_mO_n$ and $Gd_{l'}Fe_{m'}O_{n'}$ to coexist. The chemical potential of Fe, Gd or O_2 is same in both the phases. The sum of the products of the relative chemical potential and mole number of each component is equal to the standard Gibbs energy of formation of the phase. Thus,

$$l\Delta\mu(\mathrm{Gd})+m\Delta\mu(\mathrm{Fe})+n/2\Delta\mu(\mathrm{O_2}) = \Delta_f G^{\circ}(\mathrm{Gd}_l\mathrm{Fe}_m\mathrm{O}_n) \quad (34)$$

and

$$l'\Delta\mu(\mathrm{Gd})+m'\Delta\mu(\mathrm{Fe})+n'/2\Delta\mu(\mathrm{O_2}) = \Delta_f G^{\circ}(\mathrm{Gd}_{l'}\mathrm{Fe}_{m'}\mathrm{O}_{n'}). \quad (35)$$

Algebraic rearrangement yields

$$\begin{aligned}&(lm'-lm')\cdot\{\Delta\mu(\mathrm{Fe})-\Delta\mu(\mathrm{Gd})\}+\{n(m'+l')\\&\quad -n'(m+l)\}/2\cdot\Delta\mu(\mathrm{O_2})\\&=[(m'+l')\cdot\Delta_f G^{\circ}(\mathrm{Gd}_l\mathrm{Fe}_m\mathrm{O}_n)\\&\quad -(m+1)\times\Delta_f G^{\circ}(\mathrm{Gd}_{l'}\mathrm{Fe}_{m'}\mathrm{O}_{n'})]/(2.303RT).\end{aligned} \quad (36)$$

Expressing chemical potentials in terms of activities, one obtains

$$\begin{aligned}&(lm'-l'm)\log[a_{\mathrm{Gd}}/a_{\mathrm{Fe}}]+0.5\{n(m'+l')\\&\quad -n'(m+l)\}\log p(\mathrm{O_2})\\&=[(m'+l')\Delta_f G^{\circ}(\mathrm{Gd}_l\mathrm{Fe}_m\mathrm{O}_n)\\&\quad -(m+l)\Delta_f G^{\circ}(\mathrm{Gd}_{l'}\mathrm{Fe}_{m'}\mathrm{O}_{n'})]/(2.303RT).\end{aligned} \quad (37)$$

It follows from Eq. (37) that the boundaries between metallic phases ($n=n'=0$) are horizontal. Similarly, boundaries between coexisting phases in the Gd–O and Fe–O binary systems ($l=l'=0$ or $m=m'=0$) are vertical. The two-dimensional chemical potential diagram for the system Gd–Fe–O at 1250 K is shown in Fig. 11.

A disadvantage of the two-dimensional representation of chemical potentials is that absolute values of chemical potentials of the metallic components are not clearly visible. In a three-dimensional chemical potential diagram chemical potentials of each component can be explicitly shown. The three-dimensional chemical potential diagram for the system Gd–Fe–O at 1250 K is shown in Fig. 12. The stability domain of each stoichiometric phase is defined by a plane. Phases of variable composition are represented by curved surfaces. Lines, defined by the intersection of the corresponding planes, represent two-phase fields. Points of intersection of three planes represent three-phase equilibria. The chemical potential corresponding to three-phase equilibria involving the compounds $Gd_lFe_mO_n$, $Gd_{l'}Fe_{m'}O_{n'}$ and $Gd_{l''}Fe_{m''}O_{n''}$ by solving the matrix equation

$$\begin{bmatrix} l & m & n \\ l' & m' & n' \\ l'' & m'' & n'' \end{bmatrix} \begin{bmatrix} \Delta\mu(\mathrm{Gd}) \\ \Delta\mu(\mathrm{Fe}) \\ \Delta\mu(\mathrm{O}) \end{bmatrix} = \begin{bmatrix} \Delta_f G^0(\mathrm{Gd}_l\mathrm{Fe}_m\mathrm{O}_n) \\ \Delta_f G^0(\mathrm{Gd}_{l'}\mathrm{Fe}_{m'}\mathrm{O}_{n'}) \\ \Delta_f G^0(\mathrm{Gd}_{l''}\mathrm{Fe}_{m''}\mathrm{O}_{n''}) \end{bmatrix}. \quad (38)$$

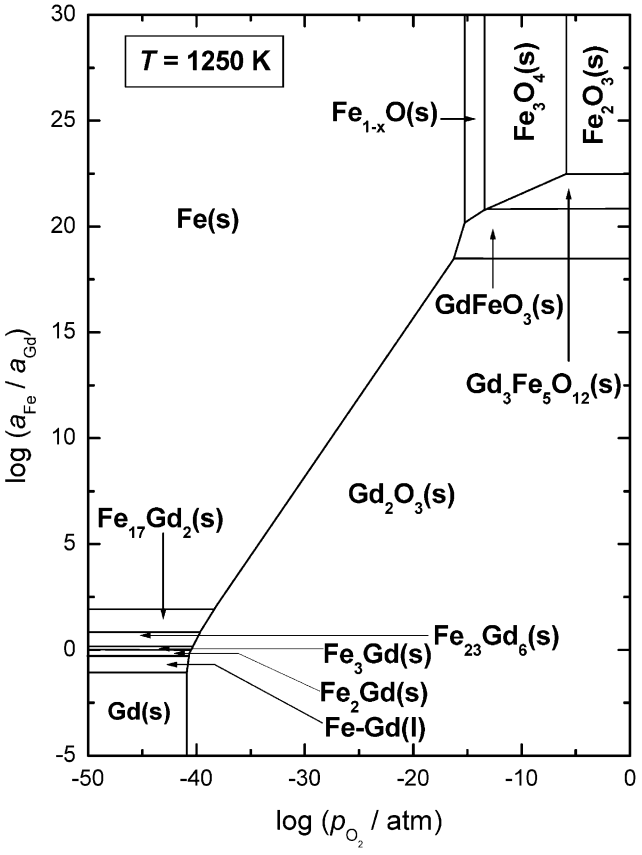

Fig. 11. Isothermal two-dimensional chemical potential diagram for the system Gd–Fe–O at 1250 K.

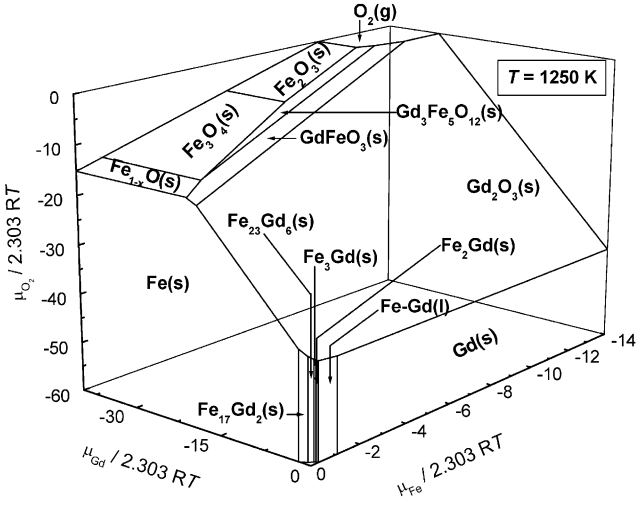

Fig. 12. Isothermal three-dimensional chemical potential diagram for the system Gd–Fe–O at 1250 K.

This equation is derived using a procedure similar to that used for deriving Eq. (37).

4. Conclusions

Ternary oxides in the systems *Ln*–Fe–O (*Ln* = Eu and Gd) have been prepared using citrate-nitrate route. The products were characterized using X-ray diffraction analysis and the particle sizes were calculated to be in the range from 2 to 4 μm. Solid-state electrochemical cells employing oxide electrolytes were used to measure the oxygen chemical potential over the coexisting phase mixtures $\{LnFeO_3(s) + Ln_2O_3(s) + Fe(s)\}$ and $\{Ln_3Fe_5O_{12}(s) + LnFeO_3(s) + Fe_3O_4(s)\}$. The Gibbs energies of formation of solid $LnFeO_3$ and $Ln_3Fe_5O_{12}$, calculated by the least-squares regression analysis of the data obtained in the present study and data for binary oxides from the literature. Isothermal oxygen potential diagrams were computed for the systems Eu–Fe–O and Gd–Fe–O at 1250 K. Isothermal chemical potential diagrams for the system Gd–Fe–O at 1250 K in two and three dimensions were computed based on the thermodynamic data obtained in this study and auxiliary data from the literature.

Acknowledgments

The authors are thankful to Dr. K. D. Singh Mudher for assisting in X-ray diffraction analysis.

References

[1] C.P. Kattak, F.F.Y. Wang, in: K.A. Gschneidner Jr., L. Eyring (Eds.), Handbook of the Physics and Chemistry of Rare Earths, North-Holland, Amsterdam, 1979, pp. 525–607.
[2] R. Pauthenet, J. Appl. Phys. 30 (1959) 290S–292S.
[3] A. Goldman, Handbook of Modern Ferromagnetic Materials, Kluwer Academic Publishers, Dordrecht, 1999, p. 207.
[4] T. Katsura, T. Sekine, K. Kitayama, T. Sugihara, N. Kimizuka, J. Solid State Chem. 23 (1978) 43–57.
[5] T. Katsura, K. Kitayama, T. Sugihara, N. Kimizuka, Bull. Chem. Soc. Japan 48 (1975) 1809–1811.
[6] Z. Singh, S. Dash, R. Prasad, D.D. Sood, J. Alloys Compd. 215 (1994) 303–307.
[7] J.N. Pratt, Metall. Trans. A 21A (1990) 1223–1250.
[8] D.A. Shores, R.A. Rapp, J. Electrochem. Soc. 118 (1971) 1107–1111.
[9] B. Sundman, J. Phase Equilibria 12 (1991) 127–140.
[10] I. Barin, Thermochemical Data of Pure Substances, Vols. I & II, 3rd ed., VCH Publishers, New York, 1995.
[11] W. Zhang, C. Li, X. Su, K. Han, J. Phase Equilibria 19 (1998) 56–63.
[12] H. Yokokawa, T. Kawada, M. Dokiya, J. Am. Ceram. Soc. 72 (1989) 2104–2110.
[13] H. Yokokawa, J. Phase Equilibria 20 (1999) 258–287.